

Distribution Voltage Regulation through Active Power Curtailment with PV Inverters and Solar Generation Forecasts

Shibani Ghosh, *Student Member, IEEE*, Saifur Rahman, *Life Fellow, IEEE*,
and Manisa Pipattanasomporn, *Senior Member, IEEE*

Abstract— Distribution voltage profiles are subjected to overvoltage limit violations from high penetration of grid-connected photovoltaic (PV) systems. Such voltage rises seen at the point of PV interconnection can be mitigated by adaptively changing the active and/or reactive power injection from the PV inverter. This work proposes a local voltage regulation technique that utilizes very short-term (15 seconds) PV power forecasts to circumvent imminent upper voltage limit violation or an overvoltage scenario. To provide these PV generation forecasts, a hybrid forecasting method is formulated based on Kalman Filter theory, which applies physical PV generation modeling using high resolution (15 seconds) data from on-site measurements. The proposed algorithm employs an active power curtailment based on these PV power forecasts, when the reactive power estimate given by a droop-based method cannot provide the desired voltage regulation within predefined power factor limits. The curtailment threshold values are calculated in such a way that this voltage regulation technique can reduce possible voltage limit violations. The effectiveness of the proposed method is demonstrated with case studies developed on a standard test feeder with realistic load and PV generation profiles.

Index Terms— High photovoltaic (PV) penetration, distribution voltage regulation, overvoltage prevention, active power curtailment, solar forecasting, Kalman Filter (KF).

I. INTRODUCTION

Solar photovoltaic (PV) energy deployment is accelerating at a rapid pace throughout the world. On a global scale, more PV capacity was added into the generation mix since 2010 than in the previous four decades [1]. As the number of PV systems interconnected to the distribution grid grows, the grid faces several opportunities as well as challenges. One of the major concerns from network operation standpoint is the overvoltage or violation of voltage limit (for example, $\pm 5\%$ of nominal voltage as given by service voltage limits of ANSI C84.1 [2]) in a distribution network due to high PV penetration. To address this issue of variable voltage rise, advanced PV inverters are being considered as a viable source of reactive power, which was not allowed under existing standards. But rapid growth of renewable sources has led to the revision of existing standards so that distributed

resources, in general, can actively participate in feeder voltage regulation when necessary [2]. Besides alleviating voltage rise, inverters can also mitigate sudden voltage drops or undervoltage scenario by capacitive VAR compensation. A local voltage regulation technique was presented by the authors in [3], which combined an inverter reactive power injection algorithm and real or active power curtailment technique to keep the voltage profile within a predefined upper threshold. In the literature, several methods are discussed to implement voltage regulation by controlling the reactive injection from the PV inverter [4-6]. Centralized control schemes use network-wide optimization to derive optimal real/reactive input set-points for inverter(s) [7-9]. However, emerging techniques like positive semidefinite optimal power flow using sparsity-promoting regularization approaches are being discussed in literature which can reduce computational burden when the voltage regulation needs to be managed on a real-time basis [8, 10]. On the other hand, decentralized or local voltage control methods can respond faster as they only involve local voltage and/or PV power production measurements [11-13], and thus can be deployed as an online application.

The reactive power capability of a PV inverter is limited by the instantaneous real power generation and its apparent power rating [4]. Consequently, the reactive power control strategies alone cannot yield sufficient voltage regulations when PV power output is high. So active power curtailment is regarded as another lucrative option with reactive power control to prevent distribution overvoltage [3, 14-15]. Besides, curtailing real power can yield in better voltage regulation given that the distribution network is resistive in nature (high R/X ratio).

Inverter-based voltage regulation applications can be further augmented by using PV generation forecasts. Solar forecasting is being used as a support tool to manage the intermittent nature of solar energy production which can lead to potential reliability concerns regarding network operation like voltage and frequency regulation [16]. Dispatching regulation reserves require short-term PV output forecasts for real-time market applications. For example, California Independent System Operator (CAISO) provides forecasts 105 minutes before the operating hour for its participating intermittent resource program [17]. The time horizon for short-term solar

The authors are with the Advanced Research Institute, and the Bradley Department of Electrical and Computer Engineering, Virginia Tech, Virginia, USA. (e-mail: shibani@vt.edu; srahman@vt.edu; mpipatta@vt.edu).

> REPLACE THIS LINE WITH YOUR PAPER IDENTIFICATION NUMBER (DOUBLE-CLICK HERE TO EDIT) <

forecasting is widely considered to be within few hours, whereas minutes timescale falls within very short-term category [18-20]. In the literature, researchers have approached the offline short-term solar generation forecasting problem using two broad types of techniques – time-series based statistical methods and artificial neural network (ANN) based techniques [21]. Statistical models rely on underlying stochastic properties of internal data structure in PV generation (direct forecasting) or solar irradiance (indirect forecasting) data [19, 21-24]. ANN methods are mostly used for indirect PV generation forecasting using training dataset, which include different weather parameters [20-21, 23, 25]. Giorgi et al presented the impact of different input variables for short-term PV power prediction in [26], where their analyses showed that the prediction accuracy improves when other measured weather parameters are taken into account, instead of only PV power and solar irradiance.

If PV generation forecasts are to be integrated with network operation applications, like local voltage regulation, it is useful to employ an online forecasting approach that does not handle a large dataset for very short-term forecasting scenario. In that case, measurement based dynamic prediction methods like Kalman Filtering (KF) technique can help reduce processing time. KF theory provides a sequential learning method that considers hourly or sub-hourly measurements for short-term PV power forecasting applications [27-30].

In this paper, a local voltage regulation technique is proposed which merges a droop-based inverter reactive power compensation algorithm and active power curtailment method using very short-term PV power forecasts. This technique expands on the local voltage regulation scheme previously developed by the authors in [3], and integrates the voltage regulation method with a hybrid forecasting algorithm that combines physical PV modeling based on KF theory. This forecasting model provides very short-term PV generation forecasts (15 seconds) that are used by this voltage regulation technique to determine required reactive compensation from the PV inverter and active power curtailment threshold. The proposed voltage regulation method is designed to be realized as an online application that can run in a smart grid environment and reduce local overvoltage under a high PV penetration scenario.

The rest of the paper is organized as follows. Section II discusses the development of the hybrid forecasting model that provides very short-term PV power forecasts. Local voltage regulation technique using the PV power forecasts is proposed in section III. The dataset and system setup for the case studies are described in section IV. Results showing the efficacy of this proposed overvoltage prevention method are presented in section V. Finally, section VI summarizes the paper with concluding remarks.

II. HYBRID FORECASTING MODEL

A hybrid forecasting model for very short-term PV generation forecasting is proposed here that combines two techniques - physical modeling of PV generation with weather parameters and application of recursive KF technique. In this

paper, very short-term PV generation forecasting is represented with 15 seconds timescale. A high-level schematic depicting this forecasting model is given in Fig. 1. As seen in Fig. 1, the forecasting model requires a physical model for PV generation which uses weather parameters. The preceding block to this generation model conditions and classifies the historical dataset according to day types and seasons. The physical PV model, provided with coarse weather forecast for the day in question, is used as an initial seed to the recursive KF application block. Based on the measurements recorded for the day, this block recalibrates the initial PV generation model to a steady-state condition once ample data is gathered. This way, the forecasting model reduces its dependence on the historical dataset and can lessen the impact of any bias present in the past dataset.

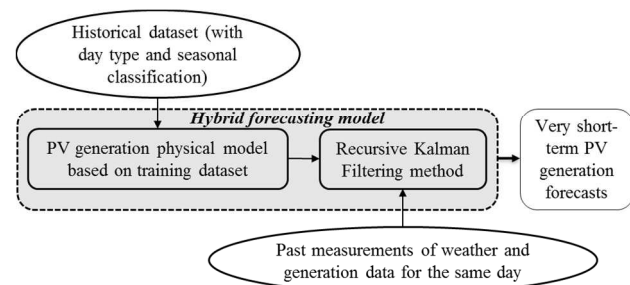


Fig. 1. High level schematic of the proposed hybrid forecasting model

A. Day type classification based on clear sky radiation model

Many research works have featured weather or day type classification for PV power forecasting method, as it helps to cluster the dataset with large variations [31-33]. These works mostly consider day types based on general weather conditions (sunny/cloudy/rainy). For this paper, a seven-group classification is assumed instead according to the incident solar energy or daily insolation (kWh/m²). This classification provides more granularity to the clustering performed on the historical dataset. Equation (1) defines the day type by the ratio (R_{dt}) between the daily measured and theoretical clear sky insolation. Clear sky radiation model used in this paper is derived using the formulae presented in [34].

$$R_{dt} = \frac{\text{measured insolation for the day}}{\text{clear sky insolation for the day}} * 100\% \quad (1)$$

The day type classifications according to the range of R_{dt} are listed in Table I. Seasonal classification is also considered in this paper (long summer: spring to fall equinox, and long winter: fall to spring equinox). Such classification yields a larger cluster for each day type in a season, compared to classification of season by winter, spring, summer, and fall.

TABLE I
DAY TYPE CLASSIFICATION ACCORDING TO AVAILABLE INSOLATION

Day type	Range of measured insolation to clear sky insolation
Sunny	$R_{dt} > 95\%$
Mostly Sunny	$85\% < R_{dt} \leq 95\%$
Partly Sunny	$70\% < R_{dt} \leq 85\%$
Partly Cloudy	$55\% < R_{dt} \leq 70\%$
Cloudy	$40\% < R_{dt} \leq 55\%$
Overcast	$25\% < R_{dt} \leq 40\%$
Snowy/rainy	$R_{dt} \leq 25\%$

This day type and seasonal classification is used to cluster daily PV generation models (described in the following section) derived from the historical dataset. An appropriate model is selected from these clusters based on the preliminary weather forecast (for the day in question) and the recursive KF process uses this model as a starting point.

B. PV generation modeling using weather parameters

Direct solar generation forecasting methods rely on the inherent non-linear relationship between the PV output power and the weather data. Researchers have investigated various input parameters to build the model for PV power [20-21, 25, 29]. To ensure the accuracy of the multivariate regression based model used in this paper, the basic physical model of PV array performance from [35] is used (Equation (2)-(4)). At maximum power point tracking (MPPT) mode, the dc voltage (V_{mp}) and current (I_{mp}) for the PV module are given by:

$$\begin{aligned} V_{mp} &= V_{mp0} + C_1 \delta(T_C) \ln(E_{irr}) + C_2 \{\delta(T_C) \ln(E_{irr})\}^2 \\ &\quad + C_3 E_{irr} \Delta T \\ I_{mp} &= I_{mp0} \{C_4 E_{irr} + C_5 E_{irr}^2\} \{1 + C_6 \Delta T\} \end{aligned} \quad (2)$$

In equation (2), V_{mp0} and I_{mp0} are the voltage and current, respectively, in MPPT mode at standard reference condition (this reference condition will be noted henceforth with subscript '0', and refers to the operating condition of solar irradiance of 1000 W/m^2 and solar cell temperature of 25°C). E_{irr} is the effective or normalized solar irradiance which is a dimensionless ratio and expressed as:

$$E_{irr} = Irr / Irr_0 \quad (3)$$

Here, Irr is the incident solar irradiance and Irr_0 is the reference irradiance ($= 1000 \text{ W/m}^2$). $\delta(T_C)$ in equation (2) is the thermal voltage per solar cell at temperature T_C which can be considered negligible (mV range per cell). ΔT denotes the difference between the cell temperature (T_C) and reference condition temperature ($T_0 = 25^\circ\text{C}$). The model coefficients C_1 to C_6 are to be determined empirically.

The average cell temperature is related to the average back-surface module temperature (T_{mdl}) and irradiance, assuming that the heat conduction through the module materials behind the cell is one-dimensional [35]. So, ΔT can be expressed in terms of T_{mdl} as:

$$\Delta T = (T_C - T_0) \approx (T_{mdl} + E_{irr} \cdot T_d) - T_0 \quad (4)$$

Here, T_d denotes predetermined temperature difference between the cell and the module temperature at the reference irradiance, Irr_0 (T_d is 3°C for the PV module considered in the case study). Combining V_{mp} and I_{mp} terms from equation (2) and neglecting the $\delta(T_C)$ components, the equation for the maximum dc power output, P_{mp} can be described as:

$$\begin{aligned} P_{mp} &= I_{mp} * V_{mp} = C_7 E_{irr} + C_8 E_{irr}^2 + C_9 E_{irr} \Delta T \\ &\quad + C_{10} E_{irr}^2 \Delta T + C_{11} E_{irr}^3 \Delta T \\ &\quad + C_{12} E_{irr}^2 \Delta T^2 \end{aligned} \quad (5)$$

Equation (5) expresses P_{mp} as a function of measurable quantities E_{irr} and ΔT . The new set of empirical coefficients

(C_7 to C_{12}) merges the previous ones (C_1 to C_6) with V_{mp0} and I_{mp0} , since both of these parameters are constant for a specific PV unit.

The module temperature in equation (4) can again be elaborated with a simplistic, empirically-developed thermal model which relates it to environmental variables- irradiance, ambient temperature and wind velocity [35]. However, the PV system considered here records temperature measurements using a sensor placed at the back of the arrays along with other weather data. These measurements are used directly for T_{mdl} for the case studies discussed in this paper. The coefficients C_7 to C_{12} are determined through regression analysis performed on the measured dataset for each day using equation (3)-(5). These coefficients represent the PV output model for the day which relates environmental variables to the solar generation. The final ac power output from the inverter is calculated from P_{mp} assuming 95.5% conversion efficiency.

C. Application of Kalman Filtering technique for PV generation forecasting

KF theory is used in this measurement based hybrid forecasting model to provide very short-term (15 seconds) PV generation forecasts. In this work, the generic mathematical relations presented by Schweppe [36] are used to apply a single-step prediction concept. For this application, the PV generation model (discussed in section II-B) is first expressed as a discrete time linear system model:

$$\mathbf{z}(n) = \mathbf{H}(n)\mathbf{x}(n) + \mathbf{v}(n) \quad (6)$$

Here, \mathbf{z} is the observation vector or measured PV generation, P_{PV} ; \mathbf{H} is the observation matrix and \mathbf{x} denotes the state vector which is comprised of the irradiance and module temperature (Equation (3)-(5)):

$$\mathbf{x}(n) = \begin{bmatrix} Irr(n) \\ T_{mdl}(n) \end{bmatrix} \quad (7)$$

The vector \mathbf{v} in equation (6) is the observation uncertainty or measurement noise, which is assumed to be zero for this forecasting model. \mathbf{H} is given by the PV generation model in equation (5) linking irradiance and module temperature to P_{PV} through intermediate variables E_{irr} and ΔT .

For time increment between adjacent samples, the state space structure in this model is described as:

$$\mathbf{x}(n+1) = \Phi(n)\mathbf{x}(n) + \mathbf{G}(n)\mathbf{w}(n) \quad (8)$$

Here, Φ is the state transition matrix, \mathbf{G} is the process noise gain matrix (assumed to be identity matrix for this particular application) and \mathbf{w} is the process noise or disturbance vector.

Theoretically, for one-step ahead prediction, the best estimate of $\mathbf{x}(n+1)$ is given by $\Phi(n)\hat{\mathbf{x}}(n|n)$. In general, $\hat{\mathbf{x}}(n_1|n_2)$ gives the best estimate of $\mathbf{x}(n_1)$, using observations $\mathbf{z}(1) \dots \mathbf{z}(n_2)$, where $n_1 > n_2$. The prediction for the next-step can then be written as:

$$\hat{\mathbf{x}}(n+1|n) = \mathbf{x}_p(n+1) = \Phi(n)\hat{\mathbf{x}}(n|n) \quad (9)$$

Here, $\mathbf{x}_p(n+1)$ denotes the predicted estimate of $\mathbf{x}(n+1)$ calculated at n^{th} time step, and $\hat{\mathbf{x}}(n|n) = \mathbf{x}_c(n)$ is the

> REPLACE THIS LINE WITH YOUR PAPER IDENTIFICATION NUMBER (DOUBLE-CLICK HERE TO EDIT) < 4

corrected estimate of $\mathbf{x}(n)$ based on the most recent observation. This correction of the state variables is done over the predicted values from the previous time step using the following relation:

$$\begin{aligned} \mathbf{x}_c(n) &= \mathbf{x}_p(n) + \mathbf{K}(n)\mathbf{e}(n) \\ \mathbf{e}(n) &= \mathbf{z}(n) - \mathbf{z}_p(n) \end{aligned} \quad (10)$$

In equation (10), $\mathbf{z}_p(n)$ is the predicted estimate of the observation parameter(s), $\mathbf{z}(n)$ ($= P_{PV}(n)$); and $\mathbf{K}(n)$ is the Kalman gain calculated at n^{th} time step. This time-varying value of Kalman gain introduces differential correction to the predicted estimate based on the output prediction error, $\mathbf{e}(n)$.

This application of KF theory to build up the PV power forecasting algorithm can thus be formulated as an iterative method with three major steps for an arbitrary time step ‘ i ’:

- *Correction:*

This part involves the correction of the predicted value as estimated from the previous iteration (equation (10)). To derive this corrected estimate, $\mathbf{x}_c(i)$ the instantaneous Kalman gain is needed which acts as a weighing parameter for the output prediction error, $\mathbf{e}(i)$. Kalman gain is expressed as:

$$\mathbf{K}(i) = \mathbf{P}_p(i)\mathbf{H}'(i)[\mathbf{H}(i)\mathbf{P}_p(i)\mathbf{H}'(i) + \mathbf{R}(i)]^{-1} \quad (11)$$

Here, $\mathbf{P}_p(i)$ is the auto covariance matrix for predicted state estimate error (derived in $(i-1)^{\text{th}}$ iteration); $\mathbf{H}(i)$ is the observation matrix evaluated at i^{th} iteration; and $\mathbf{R}(i)$ is the measurement noise covariance matrix recorded till i^{th} iteration.

- *Prediction:*

This step calculates the prediction estimates for the next time step using all the information available up to the current time instance. The predicted state estimates are derived based on the recently corrected state estimate for the current time step. Prediction for the output ($\mathbf{z}_p(i+1)$) is then given by:

$$\mathbf{z}_p(i+1) = \mathbf{H}(i)\mathbf{x}_p(i+1) \quad (12)$$

Where, $\mathbf{x}_p(i+1)$ is calculated as per equation (9) using the state transition matrix evaluated at i^{th} iteration, $\Phi(i)$.

- *Parameter update:*

The error covariance matrices are updated in this step for future use. Auto covariance matrix for predicted state estimate error is estimated by:

$$\begin{aligned} \mathbf{P}_p(i+1) &= \Phi(i)\mathbf{P}_c(i)\Phi'(i) + \mathbf{Q}(i) \\ \mathbf{P}_c(i) &= [\mathbf{I} - \mathbf{K}(i)\mathbf{H}(i)]\mathbf{P}_p(i) \end{aligned} \quad (13)$$

Here, $\mathbf{Q}(i)$ is the auto covariance matrix for process noise (\mathbf{w}) evaluated until i^{th} iteration, and $\mathbf{P}_c(i)$ is the auto covariance matrix for errors in the corrected state estimate.

The state transition matrix $\Phi(i)$ contains the transitional properties of the irradiance and module temperature as time-series data. At any time instance, the irradiance can be modeled as a product of the deterministic clear sky radiation (from section II-A) and cloud cover index. For very short-term forecasting (15 seconds), a simplistic form of $\Phi(i)$ is considered here assuming that the cloud cover index is unchanged between consecutive samples. The module temperature on the other hand, is assumed to vary in a

piecewise-linear fashion for the past minute. The initial value of the observation matrix, $\mathbf{H}(i)$, is given by the PV generation model from section II-A and II-B, (with weather type classification) based on the initial weather forecast for the day. Once ample measurement data are available and the model reaches a steady-state, $\mathbf{H}(i)$ is recalculated with the available measurements and updated for every time step (15 seconds).

III. LOCAL VOLTAGE REGULATION BASED ON PV GENERATION FORECASTS

Droop-based inverter reactive power compensation (RPC) algorithm and active power curtailment techniques (APC) are employed here to achieve local voltage regulation realized at the inverter end, as discussed in [3]. This work focuses on high PV penetration scenario where distribution overvoltage situation emerges due to reverse power flow for high PV output and low feeder load. In such case, only reactive power absorption cannot provide the desired regulation, because the R/X ratio in distribution network can be high (considering both overhead lines and cables, it can range from 0.5 to 7 for distribution network [37]), making it more sensitive to real power injection than to reactive power absorption. Therefore, curtailing active power can yield to better voltage regulation. In this study, APC is applied based on PV generation forecasts when reactive power absorption alone cannot prevent overvoltage within the predefined power factor (pf) limit. Fig. 2 shows the schematic of this combined RPC enhanced with APC based on PV forecasts technique (referred to as APCf technique in this paper), which is explained in this section.

A. Droop-based reactive power compensation (RPC)

Generic droop-based algorithm has been in vogue in power systems for power sharing and frequency control among traditional fossil-fueled generators and are now being implemented to control the real/reactive injection from inverters [3, 6, 15]. The droop-based reactive power control algorithms rely on the static Q-V relationship which is defined with piecewise linear function and the settings are location dependent [6, 11]. This linear relationship, keeping the loads at all other locations fixed, can be put as [3]:

$$\Delta Q = -Kp * \Delta V \quad (14)$$

Here, ΔQ is the estimated change in reactive load at a given bus, ΔV is the desired change in node voltage and Kp is the proportional gain or the droop parameter. Fig. 2 shows the schematic of the proposed RPC block where ΔV is specified with either $(V_{up} - Vm(i))$ or $(V_{low} - Vm(i))$. Here, $Vm(i)$ stands for the calculated node voltage (mean of three-phase voltages) at i^{th} instance, and V_{up} and V_{low} are predefined upper and lower voltage thresholds, respectively. The negative sign implies the fact that to lower the voltage by ΔV , reactive power (inductive) absorption needs to be increased by ΔQ . In other words, the inverter needs to increase its reactive power absorption in order to prevent overvoltage. The droop parameter Kp varies when the active load at the node changes. Because the solar generation can vary greatly between two adjacent time steps, a preset droop parameter might not provide the required correction in reactive compensation

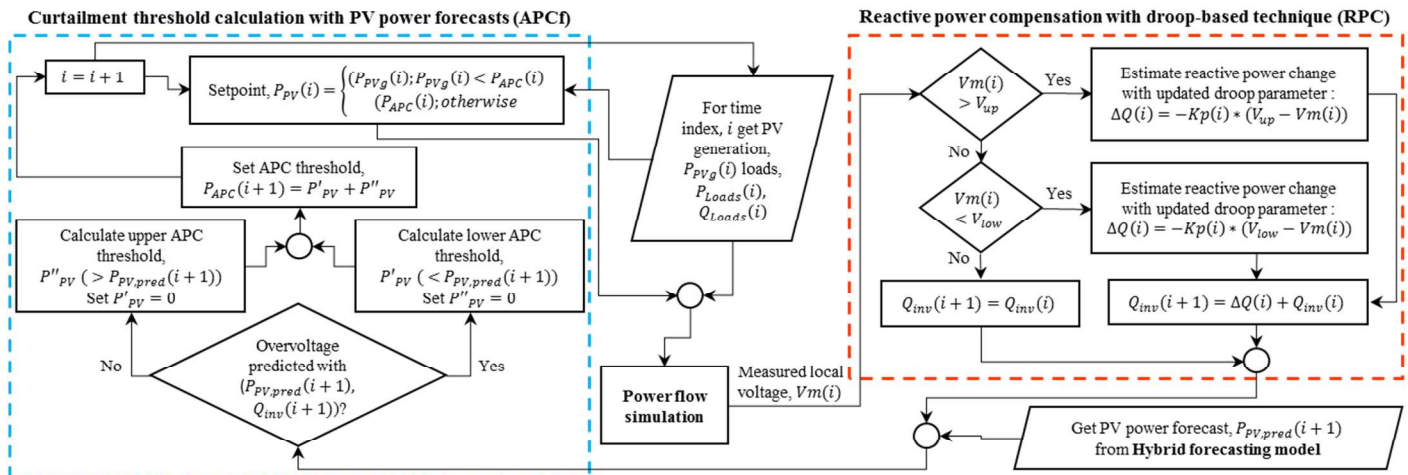


Fig. 2. Flow chart of the proposed APCf algorithm

(equation (14)). Subsequently, the proposed RPC technique updates Kp in each iteration with the actual voltage correction and preceding step change in the reactive compensation:

$$Kp(i) = \{[\Delta Q(i - 1)]\} / \{Vm(i) - Vm(i - 1)\} \quad (15)$$

This updated droop parameter helps the RPC technique to follow the changes in PV output (active) and other spot load variations. The range of Kp (corresponding maximum and minimum values) is set using the slope of Q-V contours for each bus derived from steady-state power flow analyses [3]. $\Delta Q(i)$ from equation (14) gives the estimated incremental change in inverter reactive power (Q_{inv}) for the next time step ($Q_{inv}(i + 1) = \Delta Q(i) + Q_{inv}(i)$), as seen in Fig. 2.

Positive (/negative) $Q_{inv}(i)$ denotes that the inverter acts as an inductive (/capacitive) load to the grid or absorbs(/injects) VAR. The inverter can only provide this estimated reactive power support within its reactive power capability limit, $Q_{lim}(i)$. This capability limit depends on the inverter size and thus can be expanded if the inverter is oversized compared to the maximum power rating of the PV array (P_{max} in kWp). The inverter is assumed to be oversized by 10% here, leading its apparent power rating, S (kVA) to be $1.1 * P_{max}$ [4]. Q_{lim} is primarily defined by the real power injection, P_{PV} , from a PV unit as: $\sqrt{S^2 - P_{PV}^2}$. But to maintain the power factor at the point of interconnection, this limit is redefined by the pf limit (pf_{min}). Considering both the active injection and power factor requirement, this limit is employed only after the curtailment threshold is derived. At any given time, the proposed voltage regulation technique clamps the inverter reactive power, $Q_{inv}(i)$ at $\pm Q_{lim}(i)$ if $|Q_{inv}(i)| > |Q_{lim}(i)|$.

B. Reactive power compensation enhanced with active power curtailment based on PV power forecasts (APCf)

When adequate inductive VAR absorption cannot be provided by RPC, PV output can be curtailed to prevent possible overvoltage. Although curtailing solar energy can cost the PV system owner(s), it can help avoid excess injection to the grid and thus reduce the need for grid strengthening [1, 11]. For example, Germany revised its Renewable Energy Sources Act in 2012 to oblige new PV installations (> 30 kW) to allow remote curtailment [1]. The APCf algorithm proposed

in this work, as shown in the flow chart in Fig. 2, combines APC method with RPC based on PV generation forecasts and enhances the voltage regulation performance. In practice, APCf can be implemented with constant power generation control realized at the inverter terminal which ensures a stable output level [38]. For this algorithm, active power curtailment only comes into play when an imminent overvoltage situation is being projected with the PV power forecast and estimated reactive power, or,

$$\text{Target local voltage, } Vm(P_{PV,pred}(i + 1), Q_{inv}(i + 1)) > V_{up}$$

Here, $Q_{inv}(i + 1)$ represents the required reactive power given by the RPC block, and $P_{PV,pred}(i + 1)$ gives the PV power forecast for the next time step as discussed in section II. This voltage is derived with the assumption that each PV system can access the load and generation data till the previous time step and does not have any forecast information for other PV units. This way, the local decision variables are determined independently by each PV system. Reducing active power injection decreases the target voltage and thus yield to a curtailment threshold that is lower than the predicted PV generation. Fig. 3. a) depicts the schematic for this lower threshold calculation. First, the pf limit is imposed on the estimated $Q_{inv}(i + 1)$ if $pf < pf_{min}$. The relationship between the limiting reactive power and pf limit is:

$$\begin{aligned} |Q_{lim}(i + 1)| &= W^{pf_{min}} * P_{PV,pred}(i + 1) \\ W^{pf_{min}} &= \tan(\cos^{-1}(pf_{min})) \end{aligned} \quad (16)$$

Equation (16) expresses the proportional relationship between the PV output and the reactive power limit. Here, $W^{pf_{min}}$ acts as a proportional constant which depends on the minimum

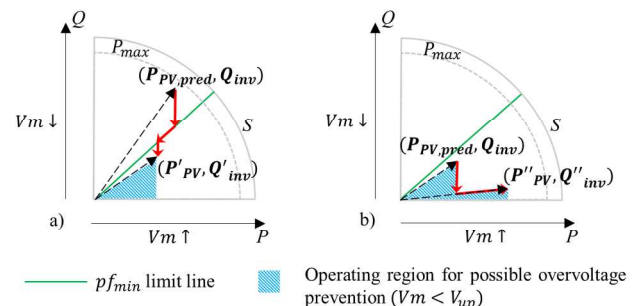


Fig. 3. a) Lower and b) upper threshold calculation for APCf

> REPLACE THIS LINE WITH YOUR PAPER IDENTIFICATION NUMBER (DOUBLE-CLICK HERE TO EDIT) <

power factor criterion specified by the grid codes. For the APC threshold calculation, as seen in Fig. 3. a), predicted real injection is reduced until it reaches an operating point (P'_{PV} and corresponding Q'_{inv}) for which the target voltage would be right under the upper voltage limit (V_{up}). These updated estimates of real and reactive power denote the lower APC threshold parameters (Equation (17)).

$$P'_{PV} \leq P_{PV,pred}(i+1); Q'_{inv} \leq W^{pf_{min}} * P'_{PV} \quad (17)$$

To make this method robust against forecasting errors, a virtual upper threshold (P''_{PV}) is calculated even when no overvoltage scenario is predicted with $P_{PV,pred}(i+1)$ and $Q_{inv}(i+1)$. This upper APC threshold calculation is thematically explained in Fig. 3. b). P''_{PV} is derived by gradually increasing the forecast value (keeping the pf fixed near unity) until the target voltage touches the upper limit. As seen in Fig. 3. b), the voltage can be increased if reactive absorption is lowered or pf is improved. So:

$$P''_{PV} > P_{PV,pred}(i+1); Q''_{inv} = 0.1 * P''_{PV} \quad (18)$$

In Fig. 3, both P'_{PV} and P''_{PV} are calculated considering the predicted PV output for the next time instance. Due to forecast errors, $P_{PV,pred}(i+1)$ can either underestimate or overestimate the actual PV generation, $P_{PVg}(i)$, leading to erroneous prediction of possible overvoltage scenario. If the overvoltage scenario is predicted properly the lower threshold calculation can help to prevent it. On the contrary, the upper threshold calculation acts as a preventive measure when an overvoltage condition is not being predicted because of the error in the PV forecast. At any instance, either upper or lower APC threshold is calculated for the next step; and the other one is set to be zero. So, net APC threshold can be written as:

$$\begin{aligned} P_{APC}(i+1) &= P'_{PV} + P''_{PV} \\ Q_{APC}(i+1) &= Q'_{inv} + Q''_{inv} \end{aligned} \quad (19)$$

The APCf technique calculates this net curtailment threshold ($P_{APC}(i+1)$) and corresponding reactive compensation ($Q_{APC}(i+1)$) adaptively based on PV power forecasts to keep the voltage within V_{up} . At any time step, 'i', $P_{APC}(i)$ acts as the curtailment threshold and if the measured PV generation, $P_{PVg}(i)$ is higher than this threshold then active power curtailment takes place. Otherwise, the instantaneous PV generation is injected without any curtailment. The PV inverter set-point ($P_{PV}(i), Q_{PV}(i)$) is:

$$\begin{aligned} P_{PV}(i), Q_{PV}(i) \\ = \min(P_{PVg}(i), P_{APC}(i)), \max(Q_{APC}(i), Q_{inv}(i)) \end{aligned} \quad (20)$$

Here, $Q_{PV}(i)$ is set as the maximum between $Q_{APC}(i)$ and $Q_{inv}(i)$ so that the reactive compensation from the inverter can be maximized within the limit ($Q_{inv}(i) \leq Q_{lim}(i)$).

IV. CASE STUDY SETUP

This work uses a modified IEEE 34-node test feeder system (Fig. 4) to build the case studies. Load profile data are derived from measurements of 1-minute resolution from a substation transformer that feeds mostly residential and commercial

customers in the Northern Virginia area. Individual spot loads at the test feeder are perturbed with Gaussian distribution (mean= scaled down base loads given by the test feeder configuration; standard deviation= 5%), to synthesize a realistic net load profile of 15 seconds resolution. Scaled base values are used for distributed loads.

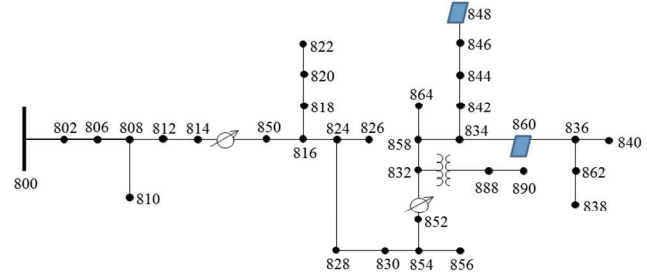


Fig. 4. Modified IEEE 34-node test feeder (PV locations at 848 & 860)

The daily PV generation profiles are derived based on real-time data collected from the 6.44 kW rooftop PV array located at Virginia Tech- Advanced Research Institute building in Arlington, Virginia (coordinates: 38.8803° N, 77.1083° W). Weather data and electrical data collected by this system are used to formulate and validate the hybrid forecasting model. System configuration data are used to model the clear sky radiation for this PV site.

As shown in Fig. 4, the PV systems are integrated at two different locations for this case study- bus#848 (PV1) and bus#860 (PV2). Bus#848 represents the end of the feeder location where the overvoltage phenomenon is most prominent [3]. To simulate high PV penetration scenario, a 700 kWp PV system is considered for PV1 and for PV2 a 300 kWp system. The PV sizing are selected in a way so that they pose similar local overvoltage scenario at the two locations. For PV1, generation profiles are scaled up from the 6.44 kW PV array data, to roughly represent any dispersed PV integration in a large-scale form. For PV2, data from another day in the month (with similar day type and irradiance/temperature profiles) is chosen and accordingly scaled up, to signify spatial variability. As this study analyzes the proposed voltage regulation technique on a very short timescale (15 seconds), the voltage regulators are operated with fixed tap positions in the 34 node test feeder. Thus, the effectiveness of the regulation technique can be assessed in absence of any other feeder voltage control device. For this case study, the proposed technique is evaluated with a narrower voltage regulation band ($V_{up} = 1.03 p.u.$ and $V_{low} = 0.97 p.u.$) compared to the standard $\pm 5\%$ range. The power factor limit is taken to be 0.9 for the oversized inverters and large-scale PV integration [6, 11]. The modified test feeder is modeled with OpenDSS. Numerical calculations regarding the hybrid forecasting model, RPC and APCf algorithms are executed in MATLAB.

The APCf technique is independently applied to each PV system which calculates the necessary reactive power compensation and the APC threshold based on the local voltage measurements and the individual forecast data.

However, it is assumed here that the PV system has access to the past load/generation data for the day through a communication infrastructure. These data are used to predict any impending local overvoltage scenario. This architecture can be visualized in a centralized fashion where each inverter sends its query to a control/data center for available load/generation data. Once these data are dispatched to the PV units, they can calculate their threshold parameters considering local injections as variables. In reality, a PV unit in one location can impact the local voltage seen by another unit, and thus the voltage can fluctuate even with locally optimized real/reactive injection. This masking effect, however, depends on the network topology, as well as the size of the PV systems, and variations in spot loads.

V. SIMULATION RESULTS

The application of the proposed APCf technique focuses on the prevention of overvoltage and thus improves the local voltage profile. This improvement shows vivid results when the feeder load is low and PV generation is high. As the feeder is located in Northern Virginia area, the net load tends to be on the lower side during Spring or March-May timeframe. To evaluate the performance of the APCf method, sample days are taken from March- May, 2013-15. Fig. 5 displays the daytime load and PV generation profiles for such a day (May 20, 2015). For the same day, Fig. 6. a) and 7. a) show the improvement in voltage profiles for PV1 and PV2 against two cases: *base case* and *modified base case*. The base case considers the actual PV generation profile without any active power curtailment or reactive power compensation (unity pf). In order to showcase a more realistic voltage control practice for comparison, the modified base case assumes constant pf operation without any curtailment. To keep it consistent with the case study presented in section IV, the pf is fixed at 0.9 for the modified base case. PV1 and PV2 voltage profiles for the base case show overvoltage situations in these figures, as they violate the upper threshold (1.03 p.u.) during peak generation hours. For the modified base case, because the reactive power compensation is limited by the pf constraint and no active power curtailment takes place, sufficient voltage regulation cannot be provided. Thus, even though the degree of overvoltage is reduced from the base case (Fig. 6. a) and 7. a)), the corresponding voltage profiles remain beyond 1.03 p.u. most of the times. In contrast, the APCf technique dynamically curtails a portion of the generated PV power, as

shown in Fig. 6. b) and 7. b), and keeps the voltage steady near about the upper limit even when the PV forecast values are not very close to the measured ones. It can be seen from Fig. 6. a) and 7. a) that, the voltage profiles for PV2 are mostly shaped by the larger PV system at the end of the feeder, PV1. Thus it needs to curtail less active power compared to PV1 (seen in Fig. 6. b) and 7. b)) even though the base case voltage profiles were showing similar overvoltage scenario. Also, both PV1 and PV2 attempt to keep their local voltages within the upper threshold independently based on their own measurements and calculations. Therefore, the actual voltage is different from their independent estimation, when both the PV systems are operating simultaneously.

To quantify the performance of the APCf technique over the day, this work uses mean overvoltage index, $\overline{V_{ov}}$ defined as:

$$\overline{V_{ov}} = \text{mean}(V_m - V_{up}); \text{ when } V_m > V_{up} \quad (21)$$

Here, V_m represents the vector containing measured voltage profile for the day, and V_{up} is the predefined upper voltage limit. The numeric values of $\overline{V_{ov}}$ (p.u.) measure the degree of the overvoltage scenario. Ideally, $\overline{V_{ov}}$ should be zero when no overvoltage is observed throughout the day. Table II shows $\overline{V_{ov}}$ values for other Spring days along with the corresponding curtailed energy (%) and forecast errors. For the forecast errors, normalized root mean square error (nRMSE %) between the PV power forecasts and generated PV power is used here as a performance evaluation criterion for the forecasting model (normalization constant = P_{max}). As seen from this table, the $\overline{V_{ov}}$'s for modified base case are less than their base case counterparts due to the reactive power compensation under a constant pf condition for all these sample days. Compared to the modified base case, the APCf technique reduces the $\overline{V_{ov}}$ indices significantly through adaptive active power curtailment and variable reactive power compensation. Also the application of the proposed APCf technique provides nearly similar improvement of the $\overline{V_{ov}}$ indices for all these days for both the PV locations. This again implies that the improvement in PV2 voltage profile is influenced by the APCf technique applied for both PV1 and PV2. The range of $\overline{V_{ov}}$ values (with APCf) indicates that the local voltage profiles remain within a moderate level of 0.005 p.u. beyond the upper threshold (V_{up}), on average, throughout the whole day. Also the $\overline{V_{ov}}$'s with APCf do not show any direct correlation with corresponding nRMSE's, proving that the technique is robust against forecasting errors.

TABLE II
MEAN OVERVOLTAGE INDICES AND RELATIVE FREQUENCIES OF OVERVOLTAGE FOR DIFFERENT DAYS

Date	Day Type	$\overline{V_{ov}}$ for Base case, PV1 (p.u.)	$\overline{V_{ov}}$ for Modified base case, PV1 (p.u.)	$\overline{V_{ov}}$ with APCf, PV1 (p.u.)	$\overline{V_{ov}}$ for Base case, PV2 (p.u.)	$\overline{V_{ov}}$ for Modified base case, PV2 (p.u.)	$\overline{V_{ov}}$ with APCf, PV2 (p.u.)	Curtailed energy with APCf, PV1 (%)	Curtailed energy with APCf, PV2 (%)	nRMSE, PV1 (%)	nRMSE, PV2 (%)
05/12/2013	Sunny	0.0194	0.0135	0.0014	0.0206	0.0149	0.0022	15.02	6.28	5.86	2.34
04/01/2014	Mostly Sunny	0.0238	0.0174	0.0043	0.0251	0.0184	0.0049	36.68	6.75	3.46	1.76
03/17/2015	Partly Sunny	0.0192	0.0139	0.0029	0.0204	0.0150	0.0036	19.59	9.27	4.85	6.09
04/29/2015	Sunny	0.0278	0.0217	0.0043	0.0292	0.0230	0.0049	42.12	7.13	2.80	2.39
05/20/2015	Sunny	0.0191	0.0125	0.0021	0.0204	0.0135	0.0031	13.91	5.28	4.27	2.34

> REPLACE THIS LINE WITH YOUR PAPER IDENTIFICATION NUMBER (DOUBLE-CLICK HERE TO EDIT) <

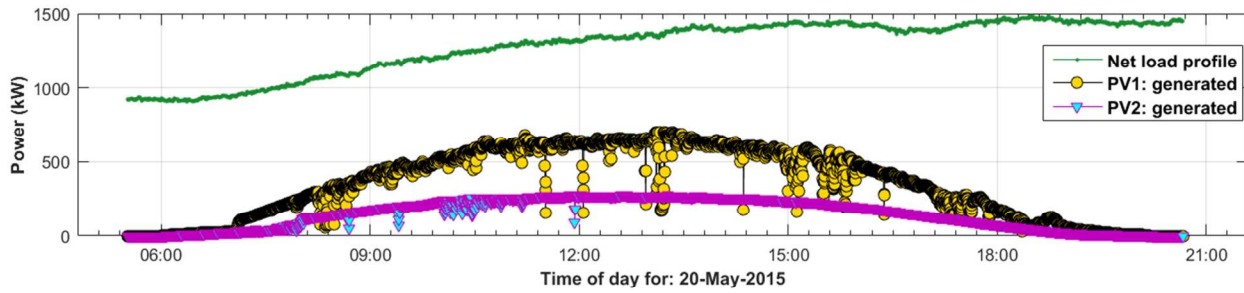


Fig. 5. Net load for the daytime and PV generation for May 20, 2015

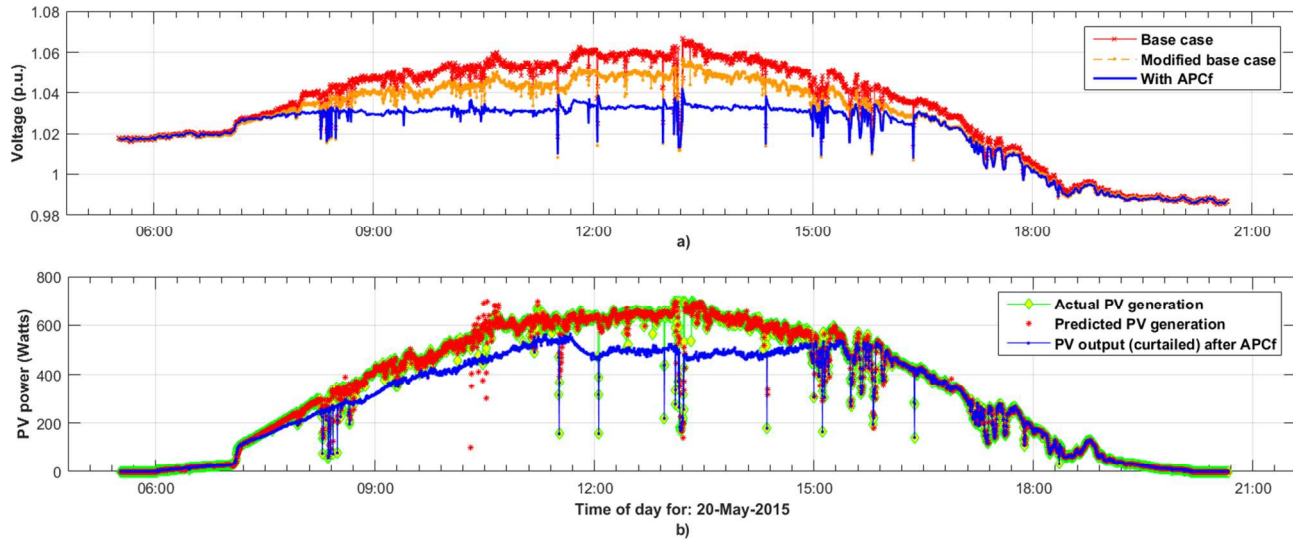


Fig. 6. a) Voltage profile improvement by APCf application over base case and modified base case, b) PV generation, prediction and output profiles (after APCf) for May 20, 2015 (for PV1)

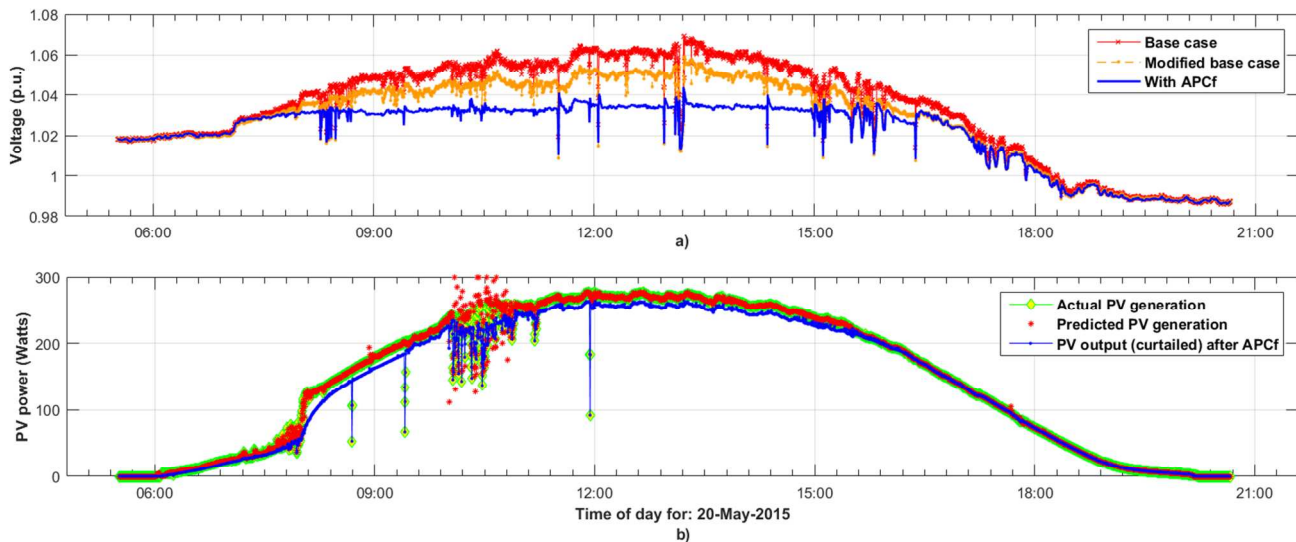


Fig. 7. a) Voltage profile improvement by APCf application over base case and modified base case, b) PV generation, prediction and output profiles (after APCf) for May 20, 2015 (for PV2)

Unlike $\overline{V_{ov}}$ with APCf, the curtailed energy is directly related to the $\overline{V_{ov}}$ for base case. High base case $\overline{V_{ov}}$ suggests that the PV generation profile is high for these days compared to the respective daily load profiles (for example: 04/01/2014, 04/29/2015). As a result, corresponding $\overline{V_{ov}}$'s for the modified base case also remain on the higher end, as no energy is curtailed under its assumptions (Table II). Higher curtailment is mandated by the APCf technique subsequently, to reduce

the extent of overvoltage for such days, for both the PV systems. However, the active power curtailment was much less for PV2, compared to PV1 (situated at the end of the feeder) even for such days. In general, PV2 does not need to curtail as much energy as PV1 because it is closer to the substation (as seen in table II). Similar findings were reported in [15] which demonstrated that the amount of curtailed energy depends on the location of the PV system (with respect

to the substation or transformer) for their droop-based active power curtailment scheme. This work modeled a residential suburban feeder with 12 houses, each having a PV system of 8.4 kWp. Their results show that the farthest houses (from the transformer) produced 15-16 kWh less than the nearest ones to the transformer, which is ~50% of the expected daily electricity generation for these houses.

The curtailed active power is also related to the power factor requirement. The closer pf_{min} is to 1 the lower the reactive power absorption/injection capability limit should be. Here, all the case studies conform to the 0.9 pf criterion. However, the proposed APCf technique is also evaluated against other hypothetical power factor criteria. Table III shows the results regarding the PV output (real and reactive) with these values of pf_{min} for PV1 (700 kWp) for May 20, 2015. The daily average curtailed power (kW) is derived by taking the mean difference between the generated (PV_{gen}) and output (PV_{out}) PV power when APC takes place ($PV_{gen} > PV_{out}$). Daily average reactive absorption (kVAR) is calculated as the mean of reactive compensation Q_{inv} when $Q_{inv} > 0$. As seen from this table, the average curtailed power increases from 10.23 kW to 24.18 kW when pf_{min} goes up from 0.8 to 0.9. The increase in active power curtailment is commensurate with the decrease in reactive compensation as it falls from 215.63 kVAR to 137.42 kVAR. This analysis infers that if the power factor requirement is relaxed, the proposed APCf technique can utilize the inverter reactive compensation capability and further reduce the necessity of active power curtailment.

TABLE III
ACTIVE POWER CURTAILMENT AND REACTIVE COMPENSATION FOR
DIFFERENT POWER FACTOR REQUIREMENT (FOR PV1: MAY 20, 2015)

pf_{min}	Average curtailed power (= $\text{mean}(PV_{gen} - PV_{out})$; when $PV_{gen} > PV_{out}$) (kW)	Average reactive compensation (= $\text{mean}(Q_{inv})$; when $Q_{inv} > 0$) (kVAR)
0.9	24.18	137.42
0.85	18.46	177.91
0.8	10.23	215.63

VI. CONCLUSION

This work proposes a local voltage regulation technique that adaptively changes real/reactive injection/absorption from the PV inverter based on PV generation forecasts to prevent distribution overvoltage, in case of high PV penetrations. The proposed voltage regulation algorithm takes aid from the very short-term (15 seconds) PV power forecasts and calculates required inverter set-points accordingly to ensure that the local voltage profile remains within the upper voltage threshold and at the same time the power factor is maintained within the predefined bounds. The PV power forecasts used for this technique are provided by a hybrid forecasting model which takes available measurements (for the given day) as inputs and uses historical dataset of the same resolution for initial weather based and seasonal clustering purpose. Using these forecast values, an imminent overvoltage scenario is predicted, while the proposed method combines a droop-based reactive power estimation method along with active power curtailment

technique to prevent such overvoltages. The proposed technique determines a virtual curtailment threshold margin along with an estimated reactive compensation, even when overvoltage is not likely to occur according to the generation forecast. In this way the performance of this method does not get hampered by instantaneous forecasting errors in case the PV forecast is much lower than the generated PV power. Case studies presented in this paper evaluate the performance of this technique for several days with varying levels of overvoltage scenarios for multiple PV systems connected to the test feeder. Results suggest that this voltage regulation technique can effectively reduce the extent of distribution overvoltage.

As this voltage regulation technique uses a forecasting method that does not involve handling of large historical dataset all the times, it can be realized as an online inverter application for addressing the voltage limit violation in distribution circuits with high PV penetrations. This technique builds upon the variable real/reactive injection/absorption capability of an inverter for maintaining the voltage within a predefined upper threshold. The method creates a framework where PV generation forecasts are used to assist the fast operation of modern smart inverters for local voltage regulation. Such an application therefore can be integrated with burgeoning smart inverter technologies to ensure seamless PV integration in a growing landscape of renewables.

REFERENCES

- [1] International Energy Agency, "Technology Roadmap: Solar Photovoltaic Energy," Sep 2014. Available: https://www.iea.org/publications/freepublications/publication/TechnologyRoadmapSolarPhotovoltaicEnergy_2014edition.
- [2] "IEEE Standard for Interconnecting Distributed Resources with Electric Power Systems - Amendment 1," *IEEE Std 1547a-2014 (Amendment to IEEE Std 1547-2003)*, pp. 1-16, May 2014.
- [3] Ghosh, S., Rahman, S., and Pipattanasomporn, M., "Local distribution voltage control by reactive power injection from PV inverters enhanced with active power curtailment," *IEEE PES General Meeting | Conference & Exposition*, pp. 1-5, National Harbor, MD, Jul 2014.
- [4] K. Turitsyn, S. Backhaus, and M. Chertkov, "Options for Control of Reactive Power by Distributed Photovoltaic Generators," *Proceedings of the IEEE*, vol. 99, no. 6, pp. 1063-1073, Jun 2011.
- [5] Tanaka, K., Oshiro, M., Toma, S., Yona, A., Senjyu, T., Funabashi, T., and Kim, C.-H., "Decentralised control of voltage in distribution systems by distributed generators," *IET Generation, Transmission & Distribution*, vol. 4, no. 11, pp. 1251-1260, Nov 2010.
- [6] Demirok, E., González, P. C., Frederiksen, K.H.B., Sera, D., Rodriguez, P., Teodorescu, R., "Local Reactive Power Control Methods for Overvoltage Prevention of Distributed Solar Inverters in Low-Voltage Grids," *IEEE Journal of Photovoltaics*, vol. 1, no. 2, pp. 174-182, 2011.
- [7] X. Su, M. Masoum, and P. Wolfs, "Optimal PV inverter reactive power control and real power curtailment to improve performance of unbalanced four-wire LV distribution networks," *IEEE Transactions on Sustainable Energy*, vol. 5, no. 3, pp. 967-977, Jul 2014.
- [8] E. Dall'Anese, S. V. Dhople, and G. B. Giannakis, "Optimal Dispatch of Photovoltaic Inverters in Residential Distribution Systems," *IEEE Transactions on Sustainable Energy*, vol. 5, no. 2, pp. 487-497, 2014.
- [9] M. Oshiro, K. Tanaka, T. Senjyu, S. Toma, A. Yona, A. Y. Saber, T. Funabashi, and C. Kim, "Optimal voltage control in distribution systems using PV generators," *International Journal of Electrical Power & Energy Systems*, vol. 33, no. 3, pp. 485-492, Mar 2011.
- [10] Baosen Zhang; Tse, D., "Geometry of injection regions of power networks," *IEEE Transactions on Power Systems*, vol. 28, no. 2, pp. 788-797, May 2013.

> REPLACE THIS LINE WITH YOUR PAPER IDENTIFICATION NUMBER (DOUBLE-CLICK HERE TO EDIT) <

10

- [11] Stetz, T., Marten, F., Braun, M., "Improved Low Voltage Grid-Integration of Photovoltaic Systems in Germany," *IEEE Transactions on Sustainable Energy*, vol. 4, no. 2, pp. 534-542, Apr 2013.
- [12] Weckx, S., Gonzalez, C., and Driesen, J., "Combined Central and Local Active and Reactive Power Control of PV Inverters," *IEEE Transactions on Sustainable Energy*, vol. 5, no. 3, pp. 776-784, Jul 2014.
- [13] A. Samadi, R. Eriksson, L. Söder, B. G. Rawn, and J. C. Boemer, "Coordinated Active Power-Dependent Voltage Regulation in Distribution Grids With PV Systems," *IEEE Transactions on Power Delivery*, vol. 29, no. 3, pp. 1454-1464, Jun 2014.
- [14] Goodwin, S.E., Krause, O., "Mitigation of voltage band violations through distributed active and reactive power control of inverter based PV generation on LV networks," *IEEE Power and Energy Society General Meeting (PES)*, pp. 1-5, Vancouver, BC, Jul 2013.
- [15] R. Tonkoski, L.A.C. Lopes, and T.H.M. El-Fouly, "Coordinated Active Power Curtailment of Grid Connected PV Inverters for Overvoltage Prevention," *IEEE Transactions on Sustainable Energy*, vol. 2, no. 2 pp. 139-147, Apr 2011.
- [16] Sioshansi, Fereidoon P., "Prospects for Renewable Energy: Meeting the Challenges of Integration with Storage", in *Smart Grid: Integrating Renewable, Distributed and Efficient Energy*, Elsevier, 2012.
- [17] North American Electric Reliability Corporation (NERC), "2013 Special Reliability Assessment: Accommodating an Increased Dependence on Natural Gas for Electric Power", May 2013. Available: http://www.nerc.com/pa/RAPA/ra/Reliability%20Assessments%20DL/NERC_PhaseII_FINAL.pdf
- [18] Lorenzo, A.T.; Holmgren, W.F.; Leuthold, M.; Chang Ki Kim; Cronin, A.D.; Betterton, E.A., "Short-term PV power forecasts based on a real-time irradiance monitoring network," *40th Photovoltaic Specialist Conference (PVSC)*, pp. 75-79, Jun 2014.
- [19] Moreno-Munoz, A., De la Rosa, J.J.G., Posadillo, R.; Bellido, F., "Very short term forecasting of solar radiation," *33rd IEEE Photovoltaic Specialists Conference (PVSC '08)*, pp. 1-5, San Diego, CA, May 2008.
- [20] J. Zeng, W. Qiao, "Short-Term Solar Power Prediction Using an RBF Neural Network," *IEEE Power and Energy Society General Meeting*, pp. 1-8, San Diego, CA, Jul 2011.
- [21] P. Bacher, H. Madsen, and H. A. Nielsen, "Online short-term solar power forecasting," *Solar Energy*, vol. 83, no. 10, pp. 1772-1783, Oct 2009.
- [22] R. Huang, T. Huang, R. Gadh, N. Li, "Solar Generation Prediction using the ARMA Model in a Laboratory-level Micro-grid," *IEEE Conf. on Smart Grid Communications (SmartGridComm)*, pp. 528-533, Nov 2012.
- [23] E. G. Kardakos, M. C. Alexiadis, S. I. Vagropoulos, C. K. Simoglou, P. N. Biskas, and A. G. Bakirtzis, "Application of Time Series and Artificial Neural Network Models in Short-term Forecasting of PV Power Generation," *48th International Universities' Power Engineering Conference (UPEC)*, Sep 2013.
- [24] C. Voyant, C. Paoli, M. Muselli, M. Nivet, "Multi-horizon solar radiation forecasting for Mediterranean locations using time series models," *Renewable and Sustainable Energy Reviews*, vol. 28, pp. 44-52, 2013.
- [25] A. Chaouachi, R.M. Kamel, R. Ichikawa, H. Hayashi, and K. Nagasaka, "Neural Network Ensemble-based Solar Power Generation Short-Term Forecasting," *World Academy of Science, Engineering and Technology*, vol. 3, 2009.
- [26] M. G. De Giorgi, P. M. Congedo, and M. Malvoni, "Photovoltaic power forecasting using statistical methods: impact of weather data," *IET Science, Measurement & Technology*, vol. 8, no. 3, pp. 90-97, May 2014.
- [27] Ciabattoni, L., Grisostomi, M., Ippoliti, G., Longhi, S., and Mainardi, E., "On line solar irradiation forecasting by minimal resource allocating networks," *20th Mediterranean Conference on Control & Automation (MED)*, pp. 1506-1511, Jul 2012.
- [28] B. Tuyishimire, R. McCann, and J. Bute, "Evaluation of a Kalman Predictor Approach in Forecasting PV Solar Power Generation," *4th IEEE International Symposium on Power Electronics for Distributed Generation Systems (PEDG)*, pp. 1-6, Jul 2013.
- [29] M. Chaabene, "Measurements based dynamic climate observer," *Solar Energy*, vol. 82, no. 9, pp. 763-771, Sep 2008.
- [30] M. Hassanzadeh, M. Etezadi-Amoli and M. S. Fadali, "Practical Approach for Sub-Hourly and Hourly Prediction of PV Power Output," *North American Power Symposium (NAPS)*, pp. 1-5, Sep 2010.
- [31] H. Yang, C. Huang, Y. Huang, Y. Pai, "A Weather-Based Hybrid Method for 1-Day Ahead Hourly Forecasting of PV Power Output," *IEEE Trans. on Sustainable Energy*, vol. 5, no. 3, pp. 917-926, Jul 2014.
- [32] C. Chen, S. Duan, T. Cai, B. Liu, "Online 24-h solar power forecasting based on weather type classification using artificial neural network," *Solar Energy*, vol. 85, no. 11, pp. 2856-2870, Nov 2011.
- [33] J. Shi, W. Lee, Y. Liu, Y. Yang, and P. Wang, "Forecasting Power Output of Photovoltaic Systems Based on Weather Classification and Support Vector Machines," *IEEE Transactions on Industry Applications*, vol. 48, no. 3, pp. 1064-1069, May/June 2012.
- [34] J. A. Duffie, W. A. Beckman, *Solar Engineering of Thermal Processes*, Second edition, John Wiley & Sons Inc., Jun 1980.
- [35] D.L. King, W.E. Boyson, J.A. Kratochvill, "Photovoltaic Array Performance Model," *Sandia Report*, 2004. Available: <http://prod.sandia.gov/techlib/access-control.cgi/2004/043535.pdf>
- [36] F. C. Schwegge, *Uncertain Dynamic Systems*, Prentice-Hall Inc., New Jersey, 1973.
- [37] Blazic, B.; Papic, I., "Voltage profile support in distribution networks — influence of the network R/X ratio," in *13th Power Electronics and Motion Control Conference 2008 EPE-PEMC*, pp. 2510-2515, Sep 2008.
- [38] Sangwongwanich, A.; Yang, Y.; Blaabjerg, F., "High-Performance Constant Power Generation in Grid-Connected PV Systems," in *IEEE Transactions on Power Electronics*, vol. 31, no. 3, pp. 1822-1825, Mar 2016.



Shibani Ghosh (S'09) received the B.Sc. degree in electrical and electronic engineering from Bangladesh University of Engineering & Technology, Bangladesh (2009), the M.S. degree in electrical engineering from Virginia Tech, USA and is currently pursuing the Ph.D. degree at Virginia Tech. She worked as a faculty member in department of electrical engineering in University of Information Technology and Sciences, Dhaka, Bangladesh in 2009-11. She is currently a Graduate Research Assistant with the Advanced Research Institute, Arlington, VA, USA. Her research interests include solar and storage integration, solar forecasting, distribution voltage control, big data analysis, power system planning and optimization techniques.



Saifur Rahman (S'75-M'78-SM'83-F'98-LF'16) received the Ph.D. degree in electrical engineering from Virginia Tech, Blacksburg, VA, USA in 1978. He is the founding director of the Advanced Research Institute, Virginia Tech, Arlington, VA, USA, where he is the Joseph R. Loring Professor of Electrical and Computer Engineering. He is also the director of the Center for Energy and the Global Environment at Virginia Tech.

Prof. Rahman is the founding Editor-in-Chief of the IEEE Electrification Magazine and the IEEE Transactions on Sustainable Energy. He is the IEEE PES President-elect for 2016 and 2017, and served as a Vice President of PES from 2009 to 2013. He is currently serving as a member of the Board of Governors of the IEEE Society on Social Implications of Technology. In 2006, he served on the IEEE Board of Directors as the Vice President for Publications. He served as the Chair of the U.S. National Science Foundation (NSF) Advisory Committee for International Science and Engineering from 2010 to 2013. He is a recipient of the IEEE Millennium Medal.



Manisa Pipattanasomporn (S'01-M'06-SM'11) received the B.S. degree in electrical engineering from Chulalongkorn University, Bangkok, Thailand (1999), the M.S. degree in energy economics and planning from the Asian Institute of Technology, Bangkok, Thailand (2001), and the Ph.D. degree in electrical engineering from Virginia Tech, USA (2004).

She joined the Department of Electrical and Computer Engineering, Virginia Tech, in 2006 and is currently an Associate Professor. She serves as one of the Principal Investigators of multiple research Grants from the U.S. National Science Foundation, the U.S. Department of Defense, and the U.S. Department of Energy, on research related to smart grid, microgrid, energy efficiency, load control, renewable energy, and electric vehicles.